

EVALUATION OF REMOTE SENSING TECHNIQUES FOR ICE-AREA CLASSIFICATION APPLIED TO THE TROPICAL QUELCCAYA ICE CAP, PERU

Todd H. Albert

*Cooperative Institute for Research in Environmental Sciences,
University of Colorado at Boulder, Boulder, Colorado 80309-0216*

Abstract: Concerns of deglaciation in the Andes prompted this investigation of methods to determine ice extent of glaciers from satellite imagery. Several remote sensing techniques to delineate ice cover are evaluated through application to the tropical Quelccaya Ice Cap. Each technique is applied to a single image that was previously geometrically and radiometrically corrected, and their results are evaluated on accuracy (as compared to a hand-digitization) and the amount of time required by a human operator to initiate and process the technique. Where the techniques require parameters, the results are shown from the best set of parameters tested. The effect of parameter selection on the results is discussed for one method. Three methods are ultimately recommended for future use with Landsat imagery. A commonly used band-ratio technique is found to be the most cost-effective method for determining ice-covered area, but the most accurate method was the supervised spectral angle mapper algorithm.

INTRODUCTION

Recent evidence suggests that 20th century warming was unprecedented in the late Holocene, and 21st century warming is projected to be much greater than the natural variability exhibited by the climate system over the past 1000 years (Houghton et al., 1996; Dyurgerov and Meier, 2000; Thompson, 2000). Observations have identified a general thinning and retreat of glaciers globally (e.g., Houghton et al., 1996; Dyurgerov and Meier, 2000; Thompson et al., 2000; Dyurgerov, 2001; Paul, 2002b), which contributes to the growing evidence of rapid global climate change.

Tropical glaciers cover an estimated 2.5×10^3 km², which corresponds to 0.16 % of the total world ice cover and 4.6% of the total area of alpine glaciers (WGMS, 1989). Over 99% of this ice-covered area occurs in the Andes, with 70 % found in Peru alone (Kaser et al., 1996). Although there is significantly more ice in high latitudes, tropical ice fields are temperate, generally existing closer to melt-threshold conditions and, accordingly, relatively small climate changes may significantly affect their mass balance (Martinson et al., 1998).

The melting of glaciers and ice caps outside of the polar regions may result in up to 23 cm of sea level rise over the next 100 years (Church et al., 2001). Furthermore, the glaciers of Peru provide critical water resources to the hyper-arid coastal lowlands and Altiplano and are also the source of glacier-related avalanches and floods that have leveled towns and caused over 35,000 recorded deaths (Williams and Ferrigno, 1999).

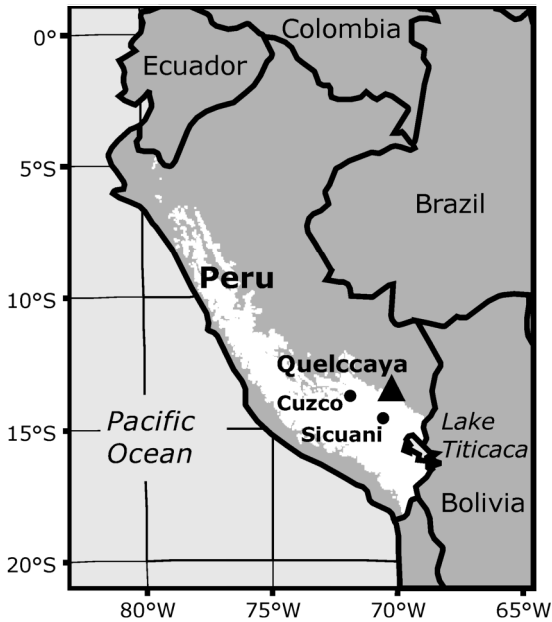


Fig. 1. Map of Peru showing the location of the Quelccaya Ice Cap. White areas are above 3500 m elevation.

Although the tropics host a number of climatic phenomena that greatly affect humans, including the El Niño–Southern Oscillation, they are characterized by relatively homogeneous thermal conditions and are not significantly affected by migratory synoptic disturbances. Accordingly, fluctuations on tropical glaciers may be more directly related to secular climate changes (Kaser and Georges, 1999). These factors make tropical glaciers exceptional indicators of recent environmental changes and the effects of these changes on natural systems (Oerlemans and Fortuin, 1992).

STUDY SITE

The largest single ice cap in the tropics, the Quelccaya Ice Cap ($13^{\circ}56'S$, $70^{\circ}50'W$, 5670 m above sea level), sits in a remote area 120 km north of Lake Titicaca and only 40 km from the Amazon rain forest (see Fig. 1). Rimmed mostly by high ice cliffs, in 1983 it had a measured ice thickness of 166 m. It feeds relatively few outlet glaciers and rests upon relatively smooth bedrock on an extensive plateau with gentle topography (Thompson et al., 1979).

Quelccaya is located in a tropical region of small annual temperature range yet pronounced seasonal precipitation differences. According to ice-core data, the average annual accumulation on Quelccaya is 1.15 m w.e./year (Thompson et al., 1985). Over 80 % of the annual precipitation falls in the summer (November through March) when solar radiation reaching the Altiplano is most intense, developing deep convective showers (Thompson et al., 1984).

The largest outlet glacier, Qori Kalis, is a valley glacier on the west side of the ice cap. Observations of its volume and extent have been made eight times since 1963

(Thompson et al., 2000). These observations indicate that the outlet glacier is retreating quickly and responds rapidly to climate forcings (Brecher and Thompson, 1993; Thompson, 2000).

REMOTE SENSING OF ALPINE GLACIERS

Satellite remote sensing is an excellent tool for monitoring isolated ice fields, as it allows more extensive and frequent observations (Gurney et al., 1993) than are otherwise available and offers a less expensive alternative to continuous field monitoring. Nevertheless, satellite sensors are still limited in their measurement resolution, and some variables cannot be observed from these platforms. Therefore, ground-based observations and field research will continue to play a crucial role in the coming years.

Topographic relief limits the application of certain remote sensors to alpine areas (Dozier et al., 1987). Remote measurements of snow and ice require similar spatial resolution to that of the topographic features. In montane areas this is on the order of tens of meters. Satellite data of this resolution are available from Landsat Thematic Mapper (TM) and from the French SPOT satellite. Although SPOT imagery has a finer pixel size, TM data have better spectral coverage, which is often important for the discrimination of land-cover classes.

In theory, the unique spectral signatures of snow and ice make them readily distinguishable from other materials in most conditions. In practice, however, the identification of snow and ice is not always straightforward. The albedo of a snow or ice surface changes dramatically with age and dustiness. This factor is especially acute near the margins, where exposed ice becomes dusty and may develop a surficial cover that resembles the surrounding glacial moraines. Additionally, snow and ice are not Lambertian; instead, their reflectance is highly dependent on the slope and aspect of the surface, the zenith angle and azimuth of the sun, and the zenith angle and azimuth of the satellite sensor. Since the geometry of the sun and satellite are effectively fixed throughout the recording of the image, additional variation in the reflectance of ice measured by the satellite may be caused by the slope and aspect of the surface. Generally, steep ice walls and crevasses in the image are heavily shaded and have very low reflectances. Shaded ice has a depressed spectral curve that approaches the spectral curve of water. Another factor that confounds the identification of ice is that edge pixels are likely to be combinations of ice and the surrounding surface material, resulting in a mixed signal.

Glacier extent mapping from satellite data has been the focus of many recent research papers. Bayr et al. (1994) used a threshold of a ratio image of TM 4 to TM 5 bands to delineate glacier area, while Rott (1994) used a threshold of a TM 3 to TM 5 ratio image. Paul (2000) found that the TM 4 to TM 5 ratio technique yielded the best results for glacier mapping on Gries Glacier, especially in regions with low insolation. Paul (2002b) estimated this method to be 95% accurate. Unsupervised classification techniques, specifically the isodata algorithm, were used to map the Southern Patagonia Ice field by Aniya et al. (1996). Supervised techniques, in combination with elevation data were used to map glaciers by Gratton et al. (1990) and by Sidjak and Wheate (1999). Fuzzy classification schemes have also been used in glacier mapping by Serandrei-Barbero et al. (1999). In this paper, each of these techniques, as well as

TABLE 1

Wavelength Ranges for Spectral Bands of the Landsat 5 TM

Landsat 5 TM	Wavelength range, μm
Band 1	0.45 - 0.52
Band 2	0.52 - 0.60
Band 3	0.63 - 0.69
Band 4	0.76 - 0.90
Band 5	1.55 - 1.75
Band 6	10.40 - 12.50
Band 7	2.08 - 2.35

some that have yet to be applied to glaciers in the literature, are compared for accuracy and processing time.

DATA DESCRIPTION

A single satellite scene was selected for use in this study. This image was acquired in the dry season (April to October) for the higher frequency of cloud-free conditions and lack of non-permanent snow cover. Still, one recent precipitation event may leave the ice and surrounding area covered with fresh snow, masking the ice extent. Accordingly, prospective images were analyzed for the presence of seasonal snow and were discarded if snow was visible on the main outlet glacier, which is typically snow-free in the dry season.

The image selected was a Landsat 5 TM image acquired July 25, 1985 and obtained from the Earth Observing System Pathfinder data set. The image was cropped to include only the ice cap and immediate environs and geometrically corrected and registered to the UTM coordinate system (zone 19 south) using a 1:25,000 scale topographic map. The satellite data were corrected for atmospheric scattering using a standard *dark object subtraction* (Chavez, 1996). This simple image-based correction is adequate for classification applications using TM data (Song et al., 2001). The data were converted to reflectance values as a final pre-processing calibration. The wavelength ranges for Landsat TM are given in Table 1.

METHODS

The 1985 image was run through a series of 16 different techniques for obtaining ice area, subsequently labeled A to P, to determine which were most cost effective. These methods include a careful hand digitization (A) of the ice area to serve as a base with which to compare all other methods. Other methods included supervised and unsupervised classification algorithms, fuzzy classification algorithms, and simple band math and threshold techniques. Each of these broad method categories was tested and is described and discussed, as are the results of the individual algorithms used.

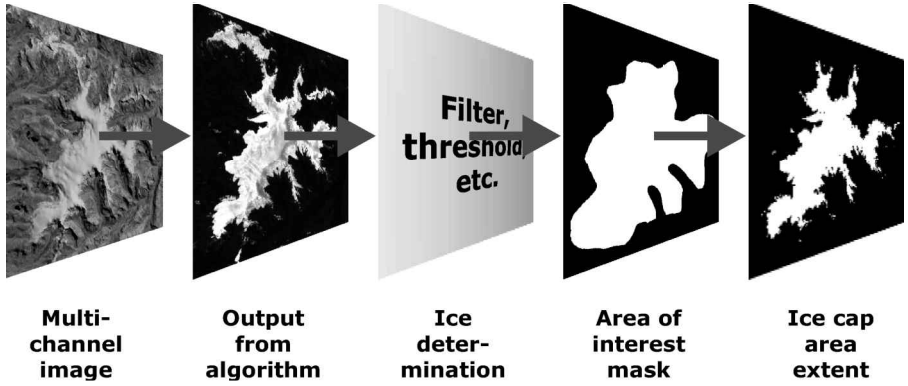


Fig. 2. Flow chart of the general processing of each technique. The product of each classification method is filtered in some way to determine ice area, and then a mask is consistently applied to all techniques so as to include only the immediate area of interest.

Techniques were ranked by both total operator time and by accuracy (Fig. 5, Table 2). Operator time does not include computer processing time, as this is becoming less and less of a concern, or the preprocessing steps which were done in all cases. Instead, the cost is associated with the additional time the operator must invest in each method, ranging here from seconds to many hours. Accuracy was determined by a comparison with a careful hand digitization. Although this is not a perfect measure of ice area, it is likely the most accurate, albeit costly, of all the methods tested. Three techniques were determined to be most cost effective and recommended for future snow and ice mapping using Landsat imagery.

Method testing

Each method was applied to the calibrated (converted to reflectances) or uncalibrated TM data where appropriate to produce a map from which total ice area is determined. A consistent mask was then applied to the results of each algorithm in order to eliminate ice area outside of the immediate area of interest, the Quelccaya Ice Cap. The resulting product is the final map of ice-covered area produced by that particular algorithm. This general procedure is illustrated in Figure 2. The ice area is calculated by multiplying the number of ice pixels by the pixel size, which is $28.5 \text{ m} \times 28.5 \text{ m}$ in this case. The final map is compared to the equivalent hand-digitized ice-area map to determine the amount of over- and under-classification. These figures are recorded in Table 2 along with the total processing time required for each method. An accuracy is estimated by adding the percent over- and under-classified ice area and subtracting the total from 100%. This penalizes the methods for both types of error.

Hand digitization

In order to estimate the accuracy of each technique, the actual areal extent of the ice cap in July 1985 was needed. It was decided that the most accurate method for determining ice-area extent was a careful *hand digitization* (A) of the ice cap from a visible

TABLE 2

Ice Area, Threshold Values for Ice,^a Processing Time, Percent Over- and Under-Classification, and Accuracy of Each Method^b

Method	Threshold value	Resulting ice area (km ²)	Estimated processing time	Over-classified ice area (%)	Under-classified ice area (%)	Estimated accuracy (%)
The control						
A. Hand Digitized		58.0	12 hours	n/a	n/a	~ 99.8
Supervised techniques						
B. Maximum Likelihood		52.0	18 min	0.4	9.4	90.2
C. Minimum Distance		43.2	15 min	0.0	24.5	75.5
D. Parallelepiped		49.8	15 min	0.0	12.9	87.1
*E. Spectral Angle Mapper (SAM)		57.7	15 min	2.1	1.2	96.7
Unsupervised techniques						
F. ISODATA		56.7	2.25 min	4.4	5.1	90.6
Fuzzy classification techniques						
G. Linear Unmixing	>0.2	58.2	16 min	5.8	4.0	90.2
H. MTMF	>0.0	47.5	16 min	1.0	17.9	81.1
I. SFF - Scatterplot vs. RMS		46.8	20 min	0.1	18.2	81.7
J. SFF	>0.5	49.8	18 min	0.5	13.3	86.2
K. MNF - PPI - MTMF - Scatterplot		47.0	2 hours	4.3	22.0	73.7
L. MNF - PPI - Linear Unmixing		49.6	2 hours	3.2	16.5	80.3
Band math and threshold techniques						
M. 3/5 Ratio	>4.0	52.6	10 sec	0.5	8.5	91.0
*N. 4/5 Ratio	>3.3	53.1	10 sec	0.5	7.5	92.0
*O. NDSI	>0.5	54.6	11 sec	0.9	5.2	93.9
P. MNF Transform	>10	52.2	1 min	0.0	8.7	91.3
Mean:		51.35	69 min	2.0	13.2	84.8

^aWhere applicable.

^bAsterisks indicate the three methods recommended for future studies (E, N, and O).

and infrared composite of the satellite image. A color composite of the 1985 satellite scene using the visible-red channel (TM 3) and two of the infrared channels (TM 4 and 5) allowed for an excellent distinction of the ice cap. This is because snow and ice have very high spectral reflectances in the visible-red (RED) and the near-infrared (NIR)

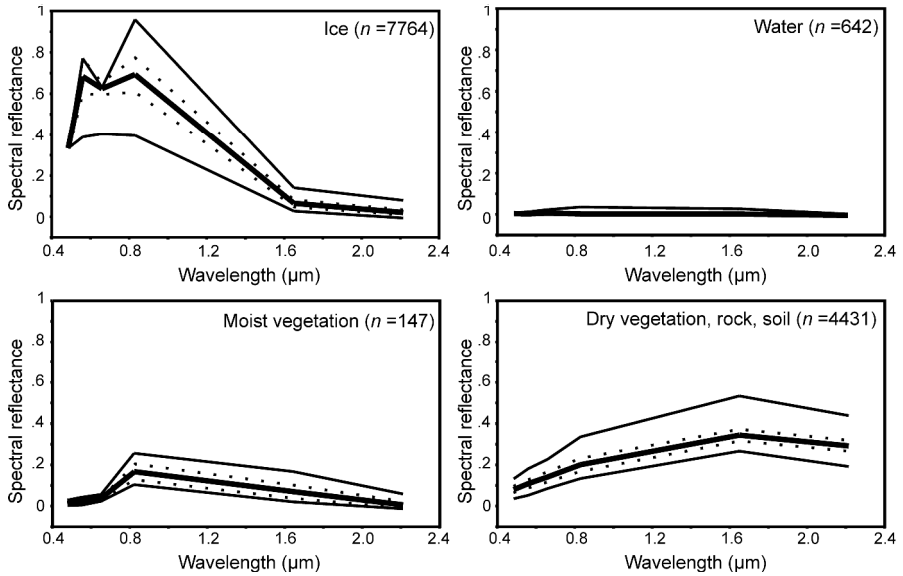


Fig. 3. Spectra from training sets used in supervised classifications. The heavy line is the mean spectral reflectance, the thinner lines are the minimum and maximum spectral reflectances, and the dotted lines are one standard deviation above and below the mean.

wavelength regions and very low spectral reflectances in the middle-infrared (MIR) wavelength region.

The ice cap was digitized on screen on a pixel-by-pixel basis. This method was extremely time-consuming and, hence, it was critical to find more cost-effective methods for determining ice-covered area. Hand digitization is, however, estimated to be greater than 99% accurate and, therefore, served as an ideal base with which to compare all other methods.

Supervised classification

Supervised classification techniques require the operator to identify known land-cover classes in the image and select image pixels that are representative of each of those classes (Mausel et al., 1990). These pixel sets are referred to as “training sets.” Generally, most of the processing time for all supervised techniques is dedicated to defining the training sets. For this study, training sets for four classes were defined. These included snow and ice, water, moist vegetation, and a mix of drier vegetation, bare rock, and soil. The statistics for these training sets are shown in Figure 3. The mean spectral reflectance and standard deviation of each land-cover class is derived from the training sets. From these training set statistics, the various supervised classification algorithms are able to select the most appropriate class for each pixel in the image (Richards and Jia, 1986).

Perhaps the most popular supervised classification algorithm is the *maximum likelihood* classifier (B). It is based on Bayesian probability theory (Eastman, 2000) and, therefore, does not assume that each pixel has equal probabilities of belonging to each

class (Hord, 1982). Instead, this algorithm utilizes the mean measurement vector and the covariance matrix from each signature to determine a probability that each pixel in an image belongs to each class. It is assumed that these statistics are normally distributed (Blaisdell, 1993). The maximum likelihood procedure is considered the most powerful hard classification system in many remote sensing applications, yet it is recommended only when the training sites are well-defined with large sample sizes and are known to be relatively homogeneous (Eastman, 2000).

A special case of the maximum likelihood classification scheme is the *minimum distance to means* (or *minimum distance*) classifier (C). By assuming identical and symmetric class distributions, the minimum distance algorithm is able to classify pixels without calculating a covariance matrix for each class (Richards and Jia, 1986). This algorithm uses the mean measurement vector of each class and places each pixel in the class to which it has the shortest Euclidean distance.

One of the simplest supervised classifiers is the *parallelepiped* classification technique (D). Parallelepiped classification defines each class as an n -dimensional parallelepiped, where n is the number of spectral bands in the image. The dimensions of the parallelepiped are defined using a threshold distance specified by the operator and the standard deviations from the mean of each class. Pixels that fall within a single class parallelepiped are assigned to that class. Pixels that do not fall within a class parallelepiped or in regions where two parallelepipeds overlap are not classified.

Although simple and efficient, this method has several shortcomings. When too small a threshold is specified, the class parallelepipeds will be small and many pixels will go unclassified. If too great a threshold is chosen, class parallelepipeds will overlap and pixels that fall in the overlapping regions are also not assigned to a class. This is especially problematic for highly correlated data sets (Richards and Jia, 1986).

The *spectral angle mapper* (SAM) algorithm (E) also treats each pixel as a vector in n -dimensional space. The spectral signature of each pixel is described by the angle its corresponding vector makes with the axes that define the n -dimensional space of the image. A mean vector for each class is calculated and all pixel vectors are classified based on the angle they make with each class vector (Richards and Jia, 1986). A maximum angle may be defined whereby pixels that are not within that angle of any class are not classified. This algorithm is less sensitive to illumination and albedo effects when used with calibrated reflectances.

The SAM classifier was applied to the calibrated data several times using a wide range of angles. The accuracy of each run is plotted against the threshold angle in Figure 4. For the image and training sets used, the highest accuracy was obtained using an angle of 0.46 radians. Estimated accuracy dropped away rapidly when angles below 0.4 radians were used, reaching 2% at an angle of 0.1 radians (not shown in Fig. 4).

Unsupervised Classification

The two greatest weaknesses of supervised classification techniques are their sensitivity to properly defined training sites and their assumption of a normally distributed probability distribution function for each class (Richards and Jia, 1986). Unsupervised classification techniques, on the other hand, use clustering techniques to

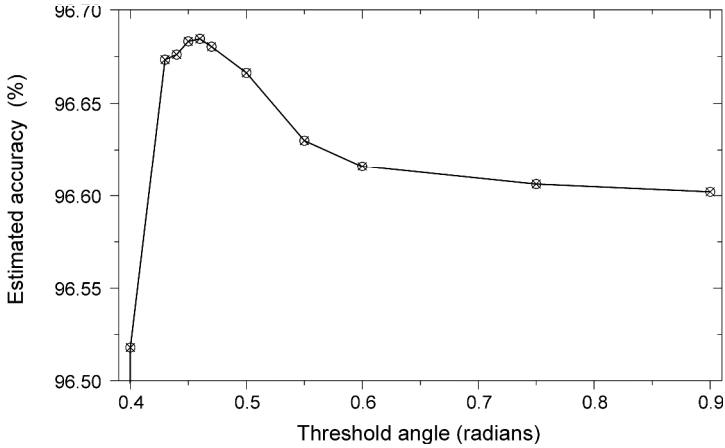


Fig. 4. Estimated accuracy is plotted against threshold angle for multiple runs of the Spectral Angle Mapper (SAM) algorithm. The best results for this study were obtained with an angle of 0.46 radians.

generate classifications by grouping pixels with similar spectral characteristics. The operator then combines and labels the spectral clusters into meaningful land cover classes (Jensen, 1996). This is not always straightforward, as clusters sometimes represent mixed classes of land cover.

The clustering method implemented here is the iterative *isodata* algorithm (F), in which candidate clusters are initially selected and their means are allowed to migrate in the spectral domain, optimizing the classification with each iteration (Ball and Hall, 1965). In each iteration of the algorithm, every pixel is compared to each cluster mean and then assigned to the nearest cluster. The means are then recalculated and the process repeats until the pixel-to-cluster mean distances are minimized or a pre-defined number of iterations is reached. The time required for class merging and labeling was found to be less than the time necessary to define training sets for the supervised classifications. The best results from the *isodata* algorithm were obtained when the algorithm was allowed to run unconstrained by a maximum number of iterations.

Fuzzy Classification Techniques

The classification techniques discussed above are considered *hard* classifiers in that all pixels are forced into discrete groups (Jensen, 1996). In reality, a single pixel is often a mixture of multiple surface types as land covers grade into one another (Lam, 1993). Fuzzy image classification uses fuzzy logic to estimate the proportions with which each class occurs in each pixel (Jensen, 1996). Several types of fuzzy classification techniques were tested. These include *linear spectral unmixing*, *mixed tuned matched filtering* (MTMF), and *spectral feature fitting* (SFF).

Linear spectral unmixing (G) is based on the assumption that the spectral reflectance of a pixel is a linear combination of the spectra of the materials present in the proportions in which they cover the pixel area (Menke, 1984). Although this technique

is better suited for hyperspectral imagery, it has been used with multispectral imagery with limited success (Richards and Jia, 1986). Linear unmixing was performed using the training classes previously defined for the supervised classifications using a threshold of 20% to define ice-covered pixels.

An additional linear spectral unmixing was performed on a training set that was established using the *endmembers*, or samples of pure cover type (Richards and Jia, 1986), established from the results of running a *pixel purity index* (PPI) algorithm. The PPI is performed on a *minimum noise fraction* (MNF) transformation of the image data (Green et al., 1988). The MNF transform is a two-step transformation. First, a *principal components analysis* (PCA) is performed on the data to decorrelate and rescale the noise. Any band-to-band correlation in the noise is removed and the resulting noise has unit variance. Next, a second PCA transformation is done on the noise-whitened data. The PPI procedure continually re-projects the MNF transform result onto random unit vectors for a user-specified number of iterations. Pixels at the ends of these vectors are tagged with each rotation. The number of times each pixel is tagged is recorded. Purer pixels tend to be tagged more often (Boardman, 1993; Boardman et al., 1995) and, thus, the highest scoring pixels are taken as potential endmembers. The 0.5% purest pixels were then rotated in 6-dimensional space to identify endmember clusters. A total of seven clusters were found and assigned to endmember training sets. A linear spectral unmixing (L) and a MTMF (K) were performed using this endmember set.

MTMF is a partial unmixing technique that does not require all image endmembers to be defined. The algorithm returns a percent cover image for each defined endmember as well as an infeasibility score for each to help reduce falsely classified pixels. For the PPI endmembers, the returned ice mixture was plotted against the infeasibility score for ice. Pixels were selected that had a high mixture score and a low infeasibility score. Visual analysis aided in determining the best thresholds to use for each. An MTMF was also run using the supervised training sets (H). Any pixel that had a positive mixture score for ice was mapped as ice-covered area.

The final fuzzy classification technique used was the SFF algorithm. This algorithm returns a scale image which is a measure of how well the spectral signature of a pixel matches each training set spectrum. A map of ice cover was created by taking all pixels as ice whose ice-mixture score was greater than 0.5 (J). The algorithm also returns a root-mean-square (RMS) error image for each training set. As an additional method, the RMS image was plotted against the ice scale image and all pixels with high scale scores and low RMS error were taken as ice (I).

Band Math and Threshold Techniques

Since the reflectivity of ice is highly dependent on the insolation and viewing angles, single spectral bands are not very successful in determining the presence or absence of ice. Multiple bands, however, are much more successful since snow and ice have such unique spectra. As such, four techniques were tested that use data from multiple bands to create a single image. A threshold is chosen whereby any pixels with values higher than the threshold are mapped as ice. The techniques included two band ratios, a Normalized Difference Snow Index (NDSI) (Kääb et al., 2002b) and an MNF transform.

Snow and ice both have high reflectances in the RED and NIR and very low reflectances in the middle infrared (MIR) region. Accordingly, band ratios of TM 3 to TM 5 and TM 4 to TM 5 are excellent indicators of snow and ice. Pixels with high 3/5 ratios (M) indicate that they have much stronger reflectances in the RED than the MIR and are likely snow or ice. A threshold of 4.0 is used on the ratio image to separate ice from all other material. Preliminary testing of this procedure on other images of Quelccaya, including images taken from SPOT 4 and Landsat 7, indicate that this threshold is quite stable and the technique may be applicable in other cases. A tremendous benefit of this method is that it requires very little operator time and is one of the most accurate methods tested.

Likewise, pixels with high 4/5 ratios (N) indicate a higher reflectance in the NIR region than the shortwave infrared (SWIR) region and likely indicate the presence of snow or ice. This ratio has been used frequently in recent literature (e.g., Paul, 2000, 2002a, 2002b; Paul et al., 2001; Kääb et al., 2002a, 2002b), and yielded better results than the 3/5 ratio. This may be due to the absorption of RED by glacial ice.

An *NDSI* (O) is based on the spectral differences of snow and ice in the visible-green wavelength region and the MIR region. It is calculated by taking the normalized difference of TM 2 and TM 5—i.e., $(TM\ 2 - TM\ 5)/(TM\ 2 + TM\ 5)$. A threshold is applied to the results to yield a map of snow and ice.

For the data used here, the first principal component derived from an *MNF transform* (P) was essentially a map of ice cover. A threshold of 10 was applied to MNF component 1 and the result was a map of ice cover comparable to the best methods tested. Further testing of this method was limited to the Quelccaya region so applicability in other areas is unknown.

RESULTS

The results of the method testing are presented in Table 2 and in Figure 5. The calculated ice area, threshold values for ice (where applicable), estimated operator time, percent over- and under-classification, and estimated accuracy for each method are provided in Table 2. Asterisks indicate the methods recommended for future work based on high accuracy and minimal processing time. The cost/benefit analysis is summarized in Figure 5. In this analysis, methods that were more accurate and required less operator time were deemed better. Points falling closer to the upper left corner of the plot, labeled “BEST,” represent techniques that are more cost effective. The methods that are recommended for future work are indicated with open circles. These include the two threshold techniques (N and O), and the SAM algorithm (E). The mean for all techniques is indicated with a large black triangle.

Figure 6 is provided for a visual comparison between the original image (false-color composite), the hand digitization (A), the most accurate method, the SAM (E), and the least accurate method presented, the MTMF using PPI endmembers (K). Of the broad method categories defined here, the threshold techniques (M–P) performed the best overall. The unsupervised classification (F) was next best in terms of cost, but more accuracy could be obtained with slightly higher cost using some of the more favorable supervised techniques. Generally, supervised classification techniques (B–E) are highly sensitive to training site definitions, so it is not surprising that the maximum likelihood classifier (B) was not outstanding in any category. Fuzzy classi-

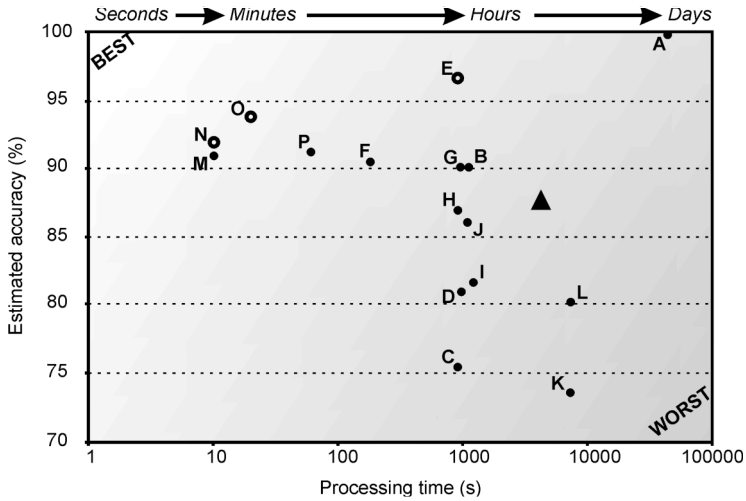


Fig. 5. Estimated accuracy is plotted against total processing time for each method used. Points falling closest to the upper-left corner (marked “BEST”) have the lowest cost/benefit ratio. Methods recommended for future applications are marked with open circles. The mean of all methods is indicated with a triangle. For the names of each method, refer to the text or to Table 2.

fication, or unmixing techniques, (G–L) are better suited for hyperspectral data, so it was surprising that one (G) outperformed the maximum likelihood classifier (B). The hand digitization (A) is estimated to be the most accurate method used, but had the highest cost by far. This method is only suitable for small glaciers.

The supervised techniques consistently did well at not over-classifying ice, but were some of the worst methods at missing ice-covered pixels. There was a fair amount of operator time for these techniques, most of which was dedicated to defining the training sites. The maximum likelihood classifier (B) did about as well as the other unsupervised techniques, but at a greater cost. The most accurate of the supervised techniques was the SAM algorithm (E). The performance of SAM, however, was highly dependent on selecting an appropriate angular threshold. In fact, the accuracy of all supervised techniques was highly dependent on the specified thresholds and generally did much better when given looser constraints. This may be partially due to the definition of a single category for snow and ice; in reality there are multiple snow and ice facies on the ice cap, each with a unique spectral signature.

The fuzzy classification (G–L) results were highly dependent on the endmember definitions. These techniques performed fairly well when endmembers were defined using the supervised training sets (G–J). In all cases, the operator time for fuzzy classifiers was primarily dedicated to the definition of endmembers. When endmembers were gathered through a PPI, the cost increased dramatically and the accuracy was quite poor. These techniques were primarily developed for hyperspectral imagery (Boardman, 1993; Boardman et al., 1995) and are not recommended for snow and ice mapping using Landsat TM imagery. None of the unmixing techniques seem to add any value and generally had higher processing costs.

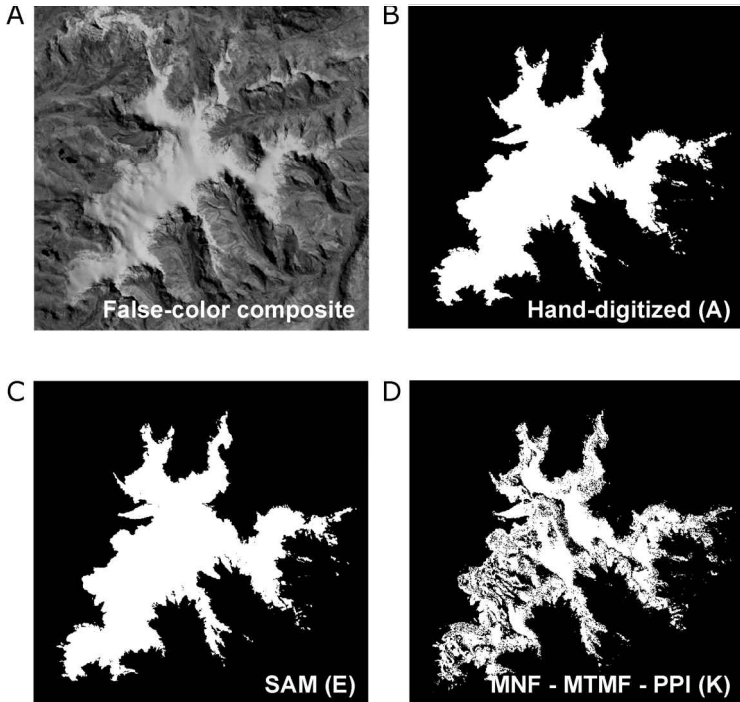


Fig. 6. False-color composite of the Quelccaya Ice Cap (A), which was used to generate (B) the hand-digitization (technique A), with an estimated accuracy of 99.8%. Shown for comparison are the results of (C) the most accurate method, the SAM (technique E) with an estimated accuracy of 96.7%, and (D) the MTMF using PPI endmembers (technique K), with an estimated accuracy of 73.7%.

The band math and threshold techniques (M–P) performed very well and had the lowest cost of all the methods tested. Each threshold techniques continued to perform well when tested with other imagery. Although all of these techniques are among the most cost effective, no benefit is seen in using a 3/5 ratio (M) or MNF (P) over the 4/5 ratio (N) or the NDSI (O). Accordingly, the latter two, along with the SAM algorithm (E), are recommended for future studies.

When dealing with ice, the most significant classification problems are often due to crevasses, moraines, and debris-covered ice. The methods that best classified these problematic areas are the same methods recommended for future analysis (Fig. 5). The maximum likelihood classifier (B) also handled these areas well. The minimum distance (C), parallelepiped (D), and MTMF techniques (H) were among the worst at dealing with these problematic pixels.

CONCLUSIONS

Aside from the high cost (in time) of the hand digitization, there are few other problems with this technique. The most significant problem is the subjective decision of which pixels to include as ice. This is less of a problem in the interior of the ice cap,

but becomes more problematic along the ice margins. Where the ice cap meets the surrounding material, pixels are more likely to be mixtures of ice and other materials. Additionally, terminal moraines at the edges of the ice cap are typically light in color and difficult to differentiate from older ice. The decision of which of these edge pixels to include as ice is somewhat discretionary and may slightly affect the resulting area. Still, any error in these decisions is random and likely accounts for only a small percent of the total ice area. For this reason, this method is used as the "control" and the accuracies of all other methods are calculated from it.

This paper aimed to report on techniques best suited for future satellite studies of ice-area extent. The results are applicable to snow and ice that is relatively free of debris. Several classification methods were subjected to a cost/benefit analysis and three were selected for future analyses. The three methods recommended for future studies are indicated by open circles in Figure 5. The methods that seem to be the most promising are the 4/5 band-ratio threshold (N) and the NDSI (O). These techniques are simple to use, fast to process, and had accurate results. SAM (E) was the most accurate of all methods tested when given a large enough threshold angle. Unlike the ratio techniques, or the NDSI, the SAM algorithm utilizes the spectral information from all bands to classify ice.

The cost/benefit analysis demonstrated that accuracy does not necessarily increase with increased cost. In fact, some methods that required the least time to process were some of the most accurate. The threshold techniques are sound examples. Overall, TM images seem adequate to determine an ice-area extent that is greater than 90 % accurate with little processing and analysis time.

LITERATURE

- Aniya, M., M. Sato, R. Naruse, P. Skvarca, and G. Casassa.** "The use of satellite and airborne imagery to inventory outlet glaciers of the Southern Patagonia Icefield, South America," *Photogrammetric Engineering and Remote Sensing*, Vol. 62, No. 12, 1996, pp. 1361-1369.
- Ball, G. H. and D. J. Hall.** *A Novel Method of Data Analysis and Pattern Classification*. Menlo Park, CA: Stanford Research Institute, 1965.
- Bayr, Klaus J., Dorothy K. Hall, and William M. Kovalick.** "Observations on glaciers in the eastern Austrian Alps using satellite data," *International Journal of Remote Sensing*, Vol. 15, No. 9, 1994, pp. 1733-1742.
- Blaisdell, E. A.** *Statistics in Practice*. New York, NY: Harcourt Brace Jovanovich, 1993.
- Boardman, J. W.** "Automated spectral unmixing of AVIRIS data using concept geometry concepts," *Proceedings from the Airborne Geosciences Workshoop*, 1993, pp. 11-14.
- Boardman, Joe W., F. A. Kruse, and R. O. Green.** "Mapping target signatures via partial unmixing of AVIRIS data," in: *Proceedings from the Airborne Geosciences Workshop*, 1995, p. 23-26.
- Brecher, Henry H. and Lonnie G. Thompson.** "Measurement of the retreat of Qori Kalis glacier in the Tropical Andes of Peru by terrestrial photogrammetry," *Photogrammetric Engineering and Remote Sensing*, Vol. 59, No. 6, 1993, pp. 1017-1022.

- Chavez, P. S.** "Image-based atmospheric corrections revisited and improved," *Photogrammetric Engineering and Remote Sensing*, Vol. 62, 1996, pp. 1025-1036.
- Church, J. A., J. M. Gregory, P. Huybrechts, M. Kuhn, K. Lambeck, M. T. Nhuan, P. Qin, P. L. Woodworth, O. A. Anisimov, F. O. Bryan, A. Cazenave, K. W. Dixon, B. B. Fitzharris, G. M. Flato, A. Ganopolski, V. Gornitz, J. A. Lowe, A. Noda, J. M. Oberhuber, S. P. O'Farrell, A. Ohmura, M. Oppenheimer, W. R. Peltier, S. C. B. Raper, C. Ritz, G. L. Russell, E. Schlosser, C. K., Shum, T. F. Stocker, R. J. Stouffer, R. S. W. van de Wal, R. Voss, E. C. Wiebe, M. Wild, D. J. Wingham, and H. J. Zwally.** "Changes in Sea Level," in J. T. Houghton, Y. Ding, D. J. Griggs, M. Noguer, P. J. van der Linden, X. Dai, K. Maskell, and C. A. Johnson, eds., *Climate Change: The Scientific Assessment*. New York, NY: Cambridge University Press, 2001, pp. 501-555.
- Dozier, Jeff, Roger Barry, Kenneth Jezek, Charles F. raymond, John Vesecky, and H. J. Zwally.** *Prospects and Concerns for Remote Sensing of Snow and Ice*. Washington, DC: National Academy of Sciences, Polar Research Board, Committee on Glaciology, Ad Hoc Panel on Remote Sensing of Snow and Ice, 1987, 31 pp.
- Dyurgerov, Mark B.** "Mountain glaciers at the end of the twentieth century: Global analysis in relation to climate and water cycle," *Polar Geography*, Vol. 25, No. 4, 2001, pp. 241-336.
- Dyurgerov, Mark B. and Mark F. Meier,** "Twentieth century climate change: Evidence from small glaciers," *Proceedings of the National Academy of Sciences*, Vol. 97, No. 4, 2000, pp. 1406-1411.
- Eastman, J. Ronald.** *Idrisi32 Help Files*. Worcester, MA: Clark Labs, The Idrisi Project, 2000.
- Gratton, D. J., P. J. Howarth, and D. J. Marceau.** "Combining DEM parameters with Landsat MSS and TM imagery in a GIS for mountain glacier characterization," *IEEE Transactions on Geoscience and Remote Sensing*, GE-28, Vol. 4, 1990, pp. 766-769.
- Green, A. A., M. Berman, P. Switzer, and M. D. Craig.** "A transformation for ordering multispectral data in terms of image quality with implications for noise removal," *IEEE Transactions on Geoscience and Remote Sensing*, Vol. 26, 1988, pp. 65-74.
- Gurney, R. J., J. L. Foster, and C. L. Parkinson.** *Atlas of Satellite Observations Related to Global Change*. Cambridge, UK: Cambridge University Press, 1993.
- Hord, R. M.** *Digital Image Processing of Remotely Sensed Data*. New York, NY: Academic Press, 1982.
- Houghton, J. T., L. G. Meira Filho, B. A. Callender, N. Harris, A. Kattenberg, and K. Maskell.** *Climate Change 1995—The IPCC Scientific Assessment*. Cambridge, UK: Cambridge University Press, 1996.
- Jensen, John R.** *Introductory Digital Image Processing: A Remote Sensing Perspective*. Englewood Cliffs, NJ: Prentice Hall, 1996.
- Kääb, Andreas, William Manely, Frank Paul, and Bruce Raup.** GLIMS Algorithm Document. GLIMS Algorithm Working Group [<http://www.geo.unizh.ch/~kaeab/glims/algorithm.html>; last updated October 11, 2002].
- Kääb, Andreas, C. Huggel, Frank Paul, R. Wessels, Bruce Raup, H. Kieffer, and J. Kargel.** Glacier monitoring from ASTER imagery: Accuracy and applications," in: *EARSel Proceedings, LIS_SIG Workshop, Berne Switzerland*, 2002.

- Kaser, Georg and Christian Georges.** "On the mass balance of low latitude glaciers with particular consideration of the Peruvian Cordillera Blanca," *Geografiska Annaler*, Vol. 81A, No. 4, 1999, pp. 643-651.
- Kaser, Georg, Stefan Hastenrath, and Alcides Ames.** "Mass balance profiles on tropical glaciers," in: *Zeitschrift für Gletscherkunde und Glazialgeologie*, 32, Measurement and Reconstruction of Glacier Mass Balance, Part 2: 75-81, 1996.
- Lam, S.** "Fuzzy sets advance spatial decision analysis," *GIS World*, Vol. 6, No. 12, 1993, pp. 58-59.
- Martinon, Douglas G. Davis S. Battisti, Raymond S. Bradley, Julia E. Cole, Rana A. Fine, Michael Ghil, Yochanan Kushnir, Michael J. Prather, Edward S. Sarachik, Pieter Tans, Lonnie G. Thompson, Michael Winton and others.** Decade-to-century-scale climate variability and change: A science strategy. Washington, DC: National Research Council, National Academy Press, Panel on Climate Variability on Decade-to-Century Time Scales, Board on Atmospheric Sciences and Climate, Commission on Geosciences, Environment, and Resources, 1998, 142 pp.
- Mausel, P. W., W. J. Kamber, and J. K. Lee.** "Optimum band selection for supervised classification of multispectral data," *Photogrammetric Engineering and Remote Sensing*, Vol. 56, No. 1, 1990, pp. 55-60.
- Menke, W.** *Geophysical Data Analysis: Discrete Inverse Theory*. San Diego, CA: Harcourt Brace Jovanovich, 1984.
- Oerlemans, J., and J. P. F. Fortuin.** "Sensitivity of glaciers and small ice caps to greenhouse warming," *Science*, Vol. 258, 1992, pp. 115-117.
- Paul, Frank.** "Evaluation of different methods for glacier mapping using Landsat TM," in: EARSeL-SIG-Workshop Land Ice and Snow. Dresden, Germany, 2000, pp. 239-245.
- Paul, Frank.** "Changes in glacier area in Tyrol, Austria, between 1969 and 1992 derived from Landsat 5 Thematic Mapper and Austrian Glacier Inventory data," *International Journal of Remote Sensing*, Vol. 23, No. 4, 2002a, pp. 787-799.
- Paul, Frank.** "Combined technologies allow rapid analysis of glacier changes," *EOS (Transactions of the American Geophysical Union)*, Vol. 83, No. 23, 2002b, pp. 253, 260-261.
- Paul, Frank, Andreas Käab, Mas Maisch, Tobias Kellenberger, and Wilfred Haerberli.** "The new remote sensing derived Swiss glacier inventory: I. Methods," in: *4th International Symposium on Remote Sensing in Glaciology*, 2001, p. 1-12.
- Richards, John A. and Xiuping Jia.** *Remote Sensing Digital Image Analysis: An Introduction*. Berlin, Germany: Springer, 1986.
- Rott, H.** "Thematic studies in alpine areas by means of polarimetric SAR and optical imagery," *Advances in Space Research*, Vol. 14, No. 3, 1994, pp. 217-226.
- Serandrei-Barbero, R., R. Rabagliati, E. Binaghi, and A. Rampini.** "Glacier retreat in the 1980s in the Breonie, Aurine and Pusteresi groups (eastern Alps, Italy) in Landsat TM images," *Hydrological Sciences Journal*, Vol. 44, No. 2, 1999, pp. 279-296.
- Sidjak, R. W. and R. D. Wheate.** "Glacier mapping of the Illecillewaet icefield, British Columbia, Canada, using Landsat TM and digital elevation data," *International Journal of Remote Sensing*, Vol. 20, No. 2, 1999, pp. 273-284.

- Song, Conghe, Curtis E. Woodcock, Karen C. Seto, Mary Pax Lenney, and Scott A. Macomber.** "Classification and change detection using Landsat TM data: When and how to correct for atmospheric effects?," *Remote Sensing of the Environment*, Vol. 75, 2001, pp. 230-244.
- Thompson, Lonnie G.** "Ice core evidence for climate change in the tropics: Implications for our future," *Quaternary Science Reviews*, Vol. 19, 2000, pp. 19-35.
- Thompson, Lonnie G., Stefan Hastenrath, and Benjamin Morales Arnao.** "Climatic ice core record from the tropical Quelccaya Ice Cap," *Science*, Vol. 203, 1979, pp. 1240-1243.
- Thompson, Lonnie G., Ellen Mosley-Thompson, J. F. Bolzan, and B. R. Koci.** "A 1500-year record of tropical precipitation in ice cores from the Quelccaya Ice Cap, Peru," *Science*, Vol. 229, No. 4717, 1985, pp. 971-973.
- Thompson, Lonnie G., Ellen Mosley-Thompson, P. M. Grootes, M. Pourchet, and S. Hastenrath.** "Tropical glaciers: Potential for ice core paleoclimatic reconstructions," *Journal of Geophysical Research*, Vol. 89, D3, 1984, pp. 4638-4646.
- Thompson, Lonnie G., Ellen Mosley-Thompson, and Keith A. Henderson.** "Ice core paleoclimate records in tropical South America since the Last Glacial Maximum," *Journal of Quaternary Science*, Vol. 15, No. 4, 2000, pp. 377-394.
- WGMS (World Glacier Monitoring Service).** *World Glacier Inventory, Status 1988*. International Association of Scientific Hydrology (ICSU)–UNEP–UNESCO, 1989.
- Williams, Richard S., Jr. and Jane G. Ferrigno.** *Satellite Image Atlas of Glaciers of the World*. Washington, DC: U.S. Government Printing Office, 1999.